Rev. LatinAm. Metal. Mat.

Artículo Regular

www.rlmm.org

STRUCTURAL CHARACTERIZATION, OPTICAL RESPONSE, AND CORROSION RESISTANCE OF BISMUTH COATINGS

José E. Alfonso[1,], Jhon J. Olaya[2], María F. Ortiz[2]*

1: Grupo de Ciencia de Materiales y Superficies, Departamento de Física, Universidad Nacional de Colombia, AA 5997 Bogotá, Colombia.

2: Departamento de Ingeniería Mecánica y Mecatrónica, Universidad Nacional de Colombia, AA 5997 Bogotá, Colombia.

**e-mail: jealfonsoo@unal.edu.co*

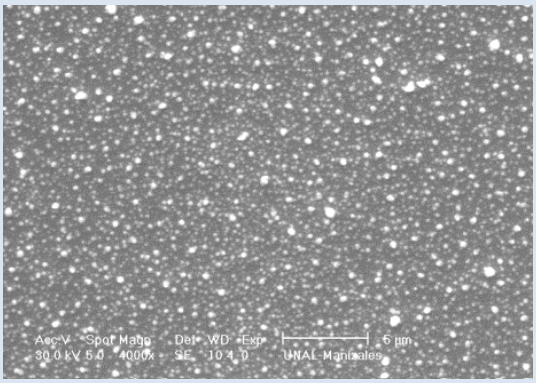

ABSTRACT

We present the results obtained from the deposition of nanostructure bismuth coatings through DC pulsed unbalanced magnetron sputtering. The Bi coatings were deposited simultaneously on common glass, silicon, and Ti6AL4V substrates in order to evaluate the optical properties, morphology, and microstructure as a function of the pulsed frequency deposition, and to establish the relationship between these properties and corrosion resistance. The microstructure was evaluated via X-ray diffraction (XRD), and the morphology of the coatings was evaluated through scanning electron microscopy (SEM) and atomic force microscopy (AFM). Optical properties were characterized through absorbance and transmittance spectra. The XRD analysis indicated that the coatings are polycrystalline. The SEM micrographs showed that the coatings are grown as droplets form. AFM revealed roughness values from 20.0 to 28.8 nm. Finally, from the optical measurements, it was possible to establish the band-gap energy of the Bi coatings.

Keywords: pulsed unbalanced magnetron sputtering, bismuth coatings, corrosion, band gap energy.

CARACTERIZACIÓN ESTRUCTURAL, RESPUESTA ÓPTICA Y RESISTENCIA A LA CORROSIÓN DE RECUBRIMIENTOS DE BISMUTO

RESUMEN

En este trabajo se presentan los resultados obtenidos en el depósito de recubrimientos nanoestructurados de Bi obtenidos mediante pulverización pulsada con magnetrón desbalanceado. Los recubrimientos de Bi fueron depositados simultáneamente sobre sustratos de vidrio común, silicio y Ti6Al4V para evaluar las propiedades ópticas, morfología y microestructura en función de la frecuencia del pulso y para establecer la relación entre estas propiedades y la resistencia a la corrosión. La estructura fue evaluada por difracción de rayos X (DRX), microscopia electrónica de barrido (MEB) y microscopía de fuerza atómica (MFA). Las propiedades ópticas fueron caracterizadas mediante espectros de absorbancia y transmitancia: El análisis de DRX indican que los recubrimientos son policristalinos. Las micrografías de MEB muestran que los recubrimientos crecen en forma columnar y gotas en la superficie. Los estudios de AFM mostraron rugosidades desde 20.0 a 28.8 nm. Finalmente, mediante las medidas ópticas fue posible establecer la brecha de energía de los recubrimientos de Bi.

Palabras clave: Pulverización pulsada desbalanceada, recubrimientos de bismuto, corrosión, brecha de energía.

Recibido: 11-12-2012 ; **Revisado:** 12-08-2013

Aceptado: 11-12-2013 ; **Publicado:** 12-12-2013

pISSN: 0255-6952 | eISSN: 2244-7113

Rev. LatinAm. Metal. Mat. 2014; **34** (2): 316-323

1. INTRODUCTION

Some authors have recently reported that bismuth is a highly anisotropic semi-metal belonging to group V [1-2] with a rhombohedral A7 crystalline structure (2 atoms per unit cell), which is typical of this group. This structure can also be described as a pseudo-cubic cell [3-4] with one atom per unit cell [5].

Moreover, Bi exhibits a thermal conductivity that is approximately one order of magnitude lower than that of typical metals, a small density of states at the Fermi level [6], a low carrier concentration, and a small effective mass (m*) [7-8]. These properties allow it to be used in various applications, such as thermoelectric devices [9], which exploit its large magnetoresistance [10] and as a reference electrode for detecting heavy metals [11-12]. Another interesting property exhibited by Bi is the transformation of films of this semi-metal into semiconductors at a critical thickness of approximately 30 nm. These films can be deposited using different techniques, such as laser pulsed deposition [1, 13], RF and DC sputtering [9, 14], and thermal evaporation [15]. Moreover, it is important to note that various authors have reported that when the coatings are deposited through physical vapor deposition (PVD) techniques, the crystalline structure and the morphology of the Bi coatings depend on such deposition parameters as the temperature of the substrate [16], the potential applied to the target [17], the ion beam energy [18], and the rate at which energy is released when the films are deposited by ion beam bombardment [19-20]. In DC sputtering, these parameters can be controlled by applying positive pulses between the substrate and the target [21], which improves film density [19, 22-23]. Similar results have been reported regarding metallic coatings (Al, Ti [24], copper [25]) and metalloid silicon targets [26] grown in an argon atmosphere.

In the present study, we investigated the microstructure, optical properties, and corrosion resistance of Bi coatings as a function of the frequency applied at the substrate using the pulsed DC sputtering technique, with the aim of evaluating its potential applications in the optical field and corrosion protection in a biological environment.

2. EXPERIMENTAL PART

Bismuth thin films were deposited simultaneously on Si [100], common glass, and Ti6Al4V alloy substrates using an unbalanced magnetron sputtering (UBM) instrument from Gencoa. The coatings on the substrates were deposited using a metallic bismuth target (99.99%) in an Ar (99.999%) atmosphere. The distance from the substrate to the target was 50 mm. The base pressure in the deposition chamber was 8 X 10^{-4} Pa, and the working pressure was 0.5 Pa, with an Ar flow of 9 sccm. The discharge power for all samples was held constant at 68 W, and the variable parameter of the deposition process was the pulse frequency (0, 40, and 80 kHz). The Bi thin films were deposited without intentional heating. The deposition time was adjusted to obtain a thickness of approximately 400 nm for all coatings.

XRD analysis was carried out with an X-PertPro Panalytical instrument in the Bragg Brentano configuration working at a current of 40 mA and voltage of 45 kV and using the K cooper monochromatic line (1.5409 A). The scanning range was from 20 to 60° with a step size of 0.02° in continuous mode. The surface morphology of the films was studied using a scanning electron microscope (XL 30 ESEM TMP), and micrographs were obtained using a mixture of secondary and backscattered electrons under high vacuum at 30 kV. Deposition rates were determined using a profilometer DEKTAK 150 at a displacement of 20 mm and an applied force of 1 mgf. The optical properties were evaluated through absorbance and transmittance measurements. Spectra were collected over a range of wavelengths between 200-600 nm using a spectrophotometer Varian Cary 5000 UV-VIS-NIR at a scan speed of 12 nm / min in 0.020 nm steps. The topography of the films was observed with electron microscope equipment JEOL model 4210 JSPM, working in tapping mode. Subsequently 3D images were obtained with the WSxM 4.0 software of the image processor scanning probe microscopy.

Corrosion tests were performed via potentiodynamic anodic polarization using a three-electrode system in a Gamry 600 potentiostat. The samples were placed at the working electrode, and a graphite rod was used as a counter electrode; a calomel-saturated electrode was used as the reference electrode. The electrolyte used was composed of 8.5 g/l NaCl, 0.25 g/l KCl, 0.22 g/l CaCl2, and 0.15 g/l NaHCO3, with a pH value of 7.8±0.1 at room temperature and an

exposed area of 0.196 cm2. This solution simulates a physiological saline solution. After 0.45 h of immersion in the corrosive solution, scans were conducted in the −400 to 9000 mV range, having a 20 mV/min potential sweep. Echem Analyst software was used for obtaining corrosion potential (Ecorr) and corrosion current (Icorr) by Tafel's extrapolation.

3. RESULTS AND DISCUSSION

To study the influence of the pulse frequency on the surface morphology and the corrosion resistance, we deposited Bi coatings on Si at different frequencies (0, 40, and 80 kHz). Figure 1 shows the deposition rate for each frequency. The results indicate that the deposition rate decreased with the frequency, and the roughness of the films doesn't show significant changes with the frequency of the deposition. The average thickness of the films was 400 nm.

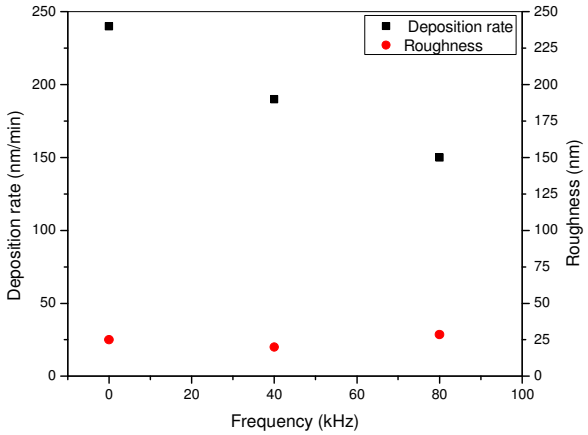

Figure 1. Deposition rate and roughness of Bi coatings as a function of the frequency.

Figure 2 shows the X-ray diffraction pattern of the Bi films deposited at different frequencies. Overall, the films were polycrystalline and exhibited peaks associated with the main planes (003), (012), (104), (015), (113), (202), and (024) corresponding to the rhombohedral phase [27] (PDF 00-005-0519). Hence the XRD pattern exhibits a higher intensity for plane (012). We calculated the ratio of texture to this plane and found the preferential growth direction [012]. Table 1 shows these values along the [012] and [003] directions and at three frequencies. The results obtained indicated that the Bi films are highly oriented along the [012] direction, in agreement with the results of other researchers [15-16, 28]. The reduction in both the thickness and texture of the coatings with the increase in the frequency could be explained by considering the fact that the ion current density increased with the frequency and generated dense plasma, which caused both the mean free path and the probability that the electron reaches the substrate to decrease [27].

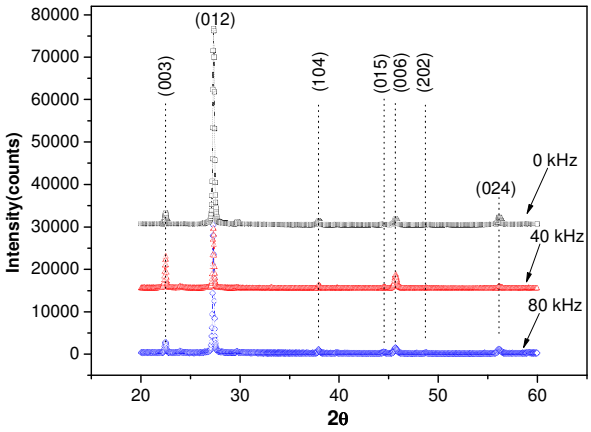

Figure 2. X-ray diffraction patterns of bismuth coatings deposited on common glass at different frequencies.

Table 1 also shows the roughness values that were obtained: the highest value was obtained for the film deposited at 80 kHz, and the lowest value was for the film grown at 40 kHz. The high roughness may be due to the difference in grain size, because there are areas with large particles and other areas where these grains are not found. The coatings deposited at 0 kHz exhibited a roughness value intermediate between the values of the films deposited at 40 and 80 kHz. This may be because the grain sizes are intermediate between those found on a smooth surface and those in areas with large particles.

Table 1. Texture coefficient and roughness values of the Bi films grown on silicon at different frequencies.

Frequencies / Planes	0 kHz	40 kHz	80 kHz
(012)	*11.73*	*12.36*	*11.16*
(003)	*7.39*	*2.56*	*10.44*
Arithmetical mean deviation Ra (nm)	*25.1*	*20.0*	*28.8*

Fig. 3 shows an SEM micrograph of a cross section of the Bi coatings deposited on (100) Si at 0 kHz. The microstructure of the films exhibits a columnar mechanism of growth, and the morphology at this

magnification seem be compact without delamination. This structure was most likely attained by the increase in the mobility of the adatoms through the transference of kinetic energy from the Bi ions that arrived at the substrate. This mechanism allows for the formation of nucleation sites, thereby reducing the number of porous and empty sites on the surface of the coatings.

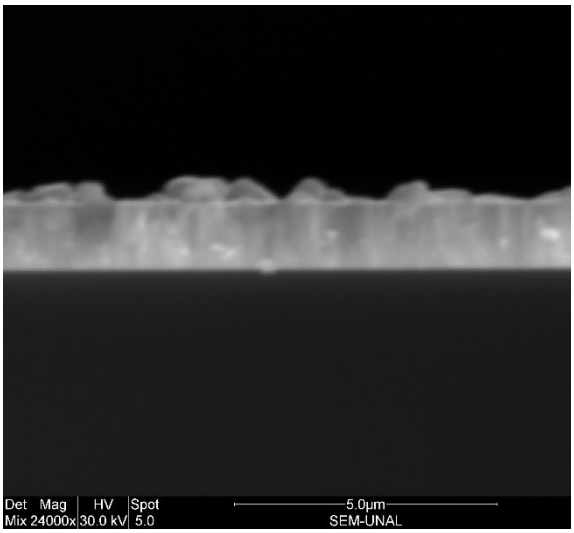

Figure 3. SEM micrograph the columnar growth of the Bi coatings deposited on silicon, at 40 kHz.

Figure 4 shows an SEM micrograph of bismuth films deposited on a silicon substrate at 0, 40 and 80 kHz. The figure shows spherical particles corresponding to bismuth, which, as verified by chemical analysis through energy dispersion spectroscopy (EDS), showed 98.12 % bismuth and 1.88% silicon from substrate in percentage of atomic weight.

These particles may be spherical, considering the fact that the melting point of bismuth is low (271.3 ºC); this quality favors the deposition of liquid droplets on the substrate surface, which can then condense [9]. The micrograph corresponding to 40 kHz shows a film with a higher density of drops and a greater number of particles with respect to the films deposited at 0 and 80 kHz.

Figure 4 also shows the grain size distribution of the films over a wide interval of 50 nm. On the film grown at 40 kHz, 3615 particles were observed, corresponding to twice the number of particles found in films grown at 0 and 80 kHz over the same area (7.30 cm^2). For the film deposited at 0 kHz, 75% featured grain sizes below 200 nm (1162 particles); the other 25% (372 particles) of the film featured grain sizes between 200 and 450 nm. Meanwhile, for the films deposited at 40 kHz, 72.5% (2621 particles) featured size grains below 200 nm, with the remaining 28% (994 particles) showing grain sizes between 200 and 450 nm. The film deposited at 80 kHz was covered with grain sizes similar to those observed for the film grown at 0 kHz (see Fig 4a.).

Regarding the optical properties, the optical absorption coefficient of the films was calculated using Equation 1 [28]. This value was squared and plotted as a function of the energy of the photons incident on the films (Fig. 5). The intercept of the tangent to the absorption curve and the energy axis allow for the determination of the energy gap of the Bi films.

$$\alpha = 2.303\, {}^{A}/_{t} \qquad (1)$$

where α is the absorption coefficient, A is the absorbance, and *t* is the thickness of the film.

The energy gaps of the Bi films deposited at frequencies of 80, 40, and 0 kHz were 4.0, 4.30, and 4.26 eV, respectively. These values are in agreement with those reported in the literature for thin films [28]. The small variation in the band gap energy may be related to the surface morphology, because a surface with large grain sizes has a greater probability of absorbing short wavelengths, whereas a surface with small size grains scatters photons and therefore absorbs short wave lengths to a lesser extent. This analysis is consistent with the results reported in morphology studies, which indicate that the film with the highest grain sizes was the film grown at 40 kHz.

Figure 6 shows the polarization potentiodynamic curves obtained in studies of the corrosion resistance of Bi films deposited on Ti6Al4V substrates at the above-mentioned frequencies.

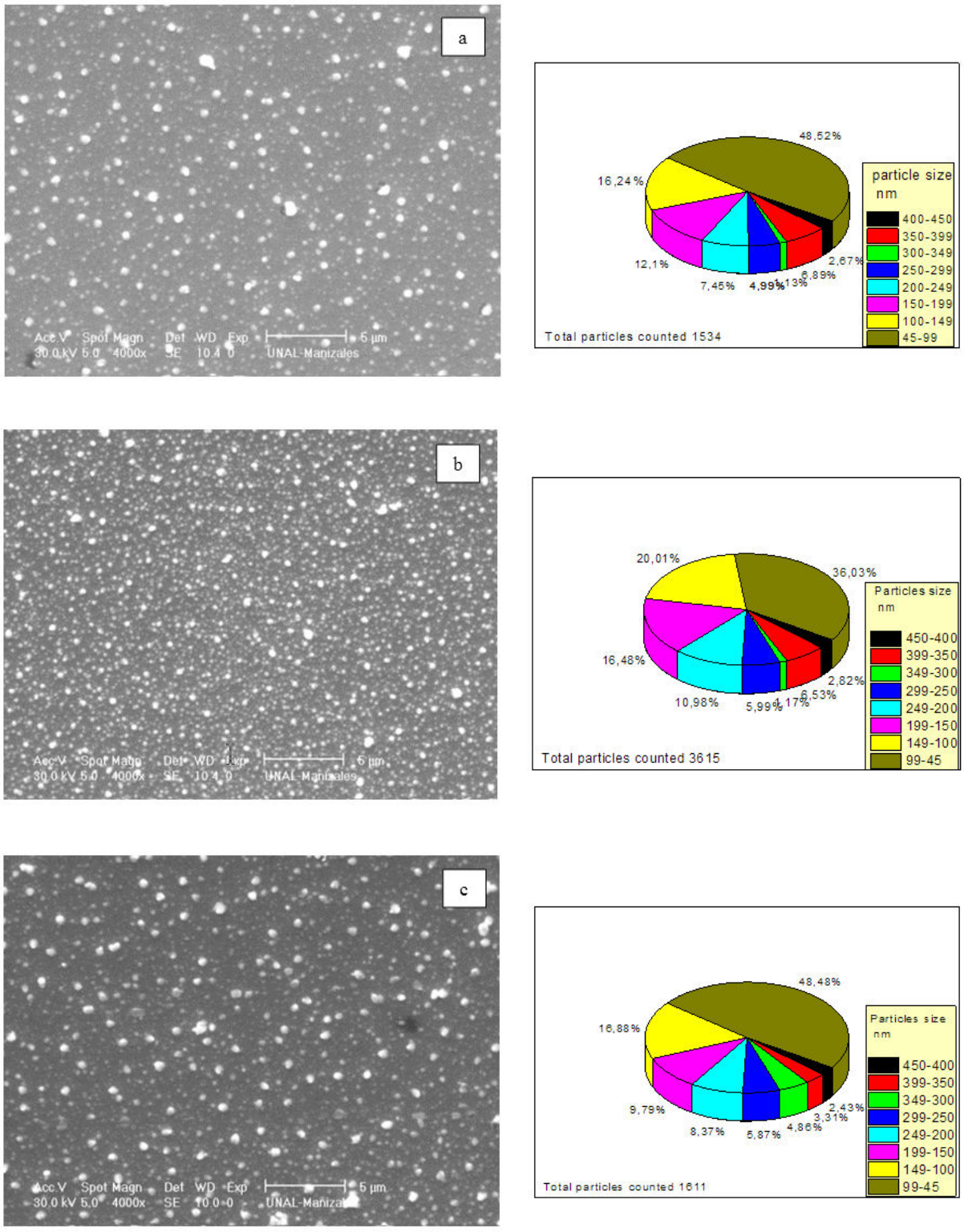

Figure 4. SEM micrographs of bismuth coating deposited at different frequencies and percentage of the grain sizes a) 0 kHz, b) 40 kHz, and c) 80 kHz.

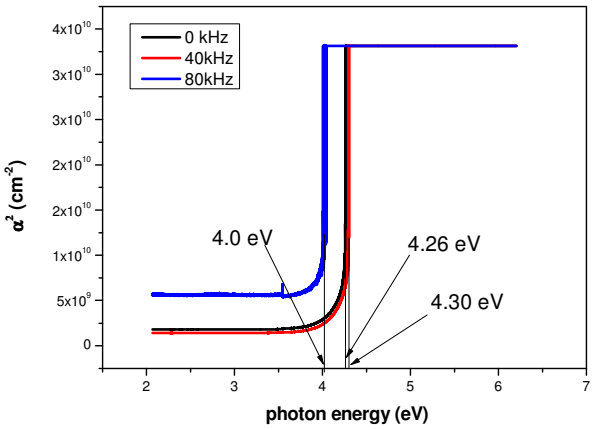

Figure 5. Variation of α^2 with photon energy for Bi coatings grown at different frequencies

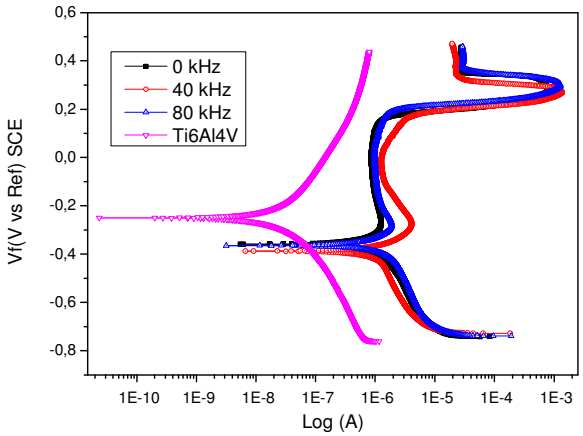

Figure 6. Polarization potentiodynamic curves of Ti6Al4V substrate and Bi coatings deposited at frequencies of 0, 40, and 80 kHz.

Corrosion resistance requires low current densities and positive corrosion potentials. Figure 6 shows that at all deposition frequencies, the Bi coatings have less corrosion resistance than the Ti6Al4V substrates. This can be explained by the oxidation of bismuth and its low adherence to the substrate. On the other hand, the morphology of the films is not compact; therefore, there are pores that allow for the diffusion of the electrolyte through the film-substrate interface, and it makes contact with the metallic substrate, causing delamination of coating. This conclusion is in agreement with the corrosion resistance results for the films, which show that the film with the lowest current density was grown at 40 kHz.

From an electrical viewpoint, the polarization potentiodynamic curve can be explained by considering different zones: zone A (Fig.7), where the cathodic behavior of the film occurs; zone B, where a change in current density that indicates the oxidation of the coating is observed; zone C, where the current density is almost constant; and zone D, where there is an activation zone, possibly due to a break in the oxidation coating and an increase in the number of pores and pinholes, which allow for the diffusion of the electrolyte in the direction of the substrate. In zone E, the corrosion density decreases the possibility of penetration of the electrolyte toward the substrate. Finally, in zone F, the current density is once again stabilized, perhaps because the measurement is made directly on the substrate.

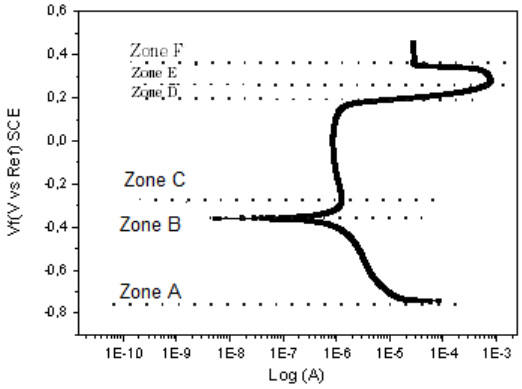

Figure 7. Potentiodynamic polarization curve of bismuth films divided by areas.

The electrical process that occurs through the above-mentioned zones can be explained by considering two chemical reactions: a cathodic reaction that occurs on the surface of the coating and an anodic reaction that occurs on the surface of the substrate. These chemical reactions can be described by the following equations:

$M - ne \rightarrow M^{n+}$ Anodic reaction

$2H_2 + 2O_2 + 4e \rightarrow 4OH^-$ Cathodic reaction or oxygen reduction

The ions and hydroxides (OH^-) that are produced by the two chemical reactions are combined in the pores of the coating to form the following compounds:

$$M^{n+} + nOH^- \rightarrow (MOH)_n$$

When the electrolyte is a salt, the metals ions react

with Cl, producing a metallic chloride (MCln); this compound reacts with water molecules to produce the following compounds:

$$MCl_n + nH_2O \rightarrow M(OH)_n + nHCl$$

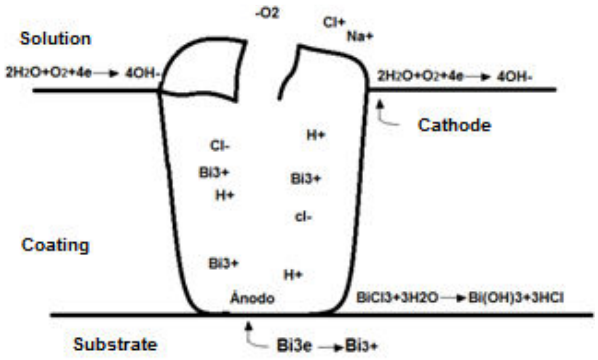

Figure 8. Chemical reactions of the corrosion process in a pinhole in a Bi film (0.9 NaCl).

Figure 8 shows the chemical reactions produced in a pinhole in a Bi film. The corrosion process and the corrosion products that accumulate in the defects of the film induce the delamination of the coating.

4. CONCLUSIONS

1.- SEM and AFM surface analysis of the deposited Bi coatings revealed different grain sizes in the particles formed at the surface; the differences among the grain sizes and their distribution were consequences of the change in the frequency at which the films were deposited.

2.- Optical absorbance studies conducted on the Bi films as a function of frequency showed that the films have high band-gap energy.

3.- Corrosion resistance studies showed that the films have less corrosion resistance than the Ti6Al4V substrate. The reduction in the corrosion resistance of the Bi coatings is possibly due to the films' granular morphology.

5. ACKNOWLEDGEMENTS

This research was carried out with financial support from European Union FP7-NMP EU-Mexico program under *grant agreement* n°263878 and the Direction the Investigation of Universidad Nacional de Colombia, Bogotá (DIB) through project No 203010016843.

6. REFERENCES

[1]. Boffoué, M. O., Lenoir, B., Scherrer, H. and Dauscher, A. Pulsed laser deposition of bismuth in the presence of different ambient atmospheres. *Thin Solid Films*, 322, 1-2 1998), 132-137.

[2]. Hattab, H., Zubkov, E., Bernhart, A., Jnawali, G., Bobisch, C., Krenzer, B., Acet, M., Möller, R. and Horn-von Hoegen, M. Epitaxial Bi(111) films on Si(001): Strain state, surface morphology, and defect structure. *Thin Solid Films*, 516, 23 2008), 8227-8231.

[3]. Chang, J., Kim, H., Han, J., Jeon, M. H. and Lee, W. Y. Microstructure and magnetoresistance of sputtered bismuth thin films upon annealing. *Journal of Applied Physics*, 98, 2 2005), 023906.

[4]. Vereecken, P. M., Sun, L., Searson, P. C., Tanase, M., Reich, D. H. and Chien, C. L. Magnetotransport properties of bismuth films on p-GaAs. *Journal of Applied Physics*, 88, 11 2000), 6529-6535.

[5]. Ph, H. The surfaces of bismuth: Structural and electronic properties. *Progress in Surface Science*, 81, 5 2006), 191-245.

[6]. Mönig, H., Sun, J., Koroteev, Y. M., Bihlmayer, G., Wells, J., Chulkov, E. V., Pohl, K. and Hofmann, P. Structure of the (111) surface of bismuth: LEED analysis and first-principles calculations. *Physical Review B*, 72, 8 2005), 085410.

[7]. Ast, C. R. and Höchst, H. Fermi Surface of Bi(111) Measured by Photoemission Spectroscopy. *Physical Review Letters*, 87, 17 2001), 177602.

[8]. Hirahara, T., Nagao, T., Matsuda, I., Bihlmayer, G., Chulkov, E. V., Koroteev, Y. M. and Hasegawa, S. Quantum well states in ultrathin Bi films: Angle-resolved photoemission spectroscopy and first-principles calculations study. *Physical Review B*, 75, 3 2007), 035422.

[9]. Kim, D.-H., Lee, S.-H., Kim, J.-K. and Lee, G.-H. Structure and electrical transport properties of bismuth thin films prepared by RF magnetron sputtering. *Applied Surface Science*, 252, 10 2006), 3525-3531.

[10]. Mangez, J. H., Issi, J. P. and Heremans, J. Transport properties of bismuth in quantizing magnetic fields. *Physical Review B*, 14, 10 1976), 4381-4385.

[11]. Hutton, E. A., Ogorevc, B., Hočevar, S. B., Weldon, F., Smyth, M. R. and Wang, J. An introduction to bismuth film electrode for use in cathodic electrochemical detection. *Electrochemistry Communications*, 3, 12 2001),

707-711.

[12]. Pauliukaitė, R., Hočevar, S. B., Ogorevc, B. and Wang, J. Characterization and Applications of a Bismuth Bulk Electrode. *Electroanalysis*, 16, 9 2004), 719-723.

[13]. Jacquot, A., Boffoué, M. O., Lenoir, B. and Dauscher, A. The effect of different scanning schemes on target and film properties in pulsed laser deposition of bismuth. *Applied Surface Science*, 156, 1–4 2000), 169-176.

[14]. Hsu, J.-H., Wang, H.-X. and Kuo, P. C. Evolution of magnetoresistance effect in iron–bismuth films. *Journal of Magnetism and Magnetic Materials*, 294, 2 2005), e99-e103.

[15]. Kumari, L., Lin, S.-J., Lin, J.-H., Ma, Y.-R., Lee, P.-C. and Liou, Y. Effects of deposition temperature and thickness on the structural properties of thermal evaporated bismuth thin films. *Applied Surface Science*, 253, 14 2007), 5931-5938.

[16]. Dauscher, A., Boffoué, M. O., Lenoir, B., Martin-Lopez, R. and Scherrer, H. Unusual growth of pulsed laser deposited bismuth films on Si(100). *Applied Surface Science*, 138-139, 0 1999), 188-194.

[17]. Jeffrey, C. A., Zheng, S. H., Bohannan, E., Harrington, D. A. and Morin, S. X-ray characterization of as-deposited, epitaxial films of Bi(012) on Au(111). *Surface Science*, 600, 1 2006), 95-105.

[18]. Mammeri, S., Ouichaoui, S., Ammi, H. and Zemih, R. Sputtering and crystalline structure modification of bismuth thin films deposited onto silicon substrates under the impact of 20–160 keV Ar+ ions. *Nuclear Instruments and Methods in Physics Research Section B: Beam Interactions with Materials and Atoms*, 268, 2 2010), 140-148.

[19]. Arnell, R. D., Kelly, P. J. and Bradley, J. W. Recent developments in pulsed magnetron sputtering. *Surface and Coatings Technology*, 188-189, 0, 158-163.

[20]. Kelly, P. J. and Arnell, R. D. Control of the structure and properties of aluminum oxide coatings deposited by pulsed magnetron sputtering. *Journal of Vacuum Science & Technology A: Vacuum, Surfaces, and Films*, 17, 3 1999), 945-953.

[21]. Bradley, J. W., Bäcker, H., Kelly, P. J. and Arnell, R. D. Space and time resolved Langmuir probe measurements in a 100 kHz pulsed rectangular magnetron system. *Surface and Coatings Technology*, 142-1442001), 337-341.

[22]. Lin, J., Moore, J. J., Mishra, B., Sproul, W. D. and Rees, J. A. Examination of the pulsing phenomena in pulsed-closed field unbalanced magnetron sputtering (P-CFUBMS) of Cr–Al–N thin films. *Surface and Coatings Technology*, 201, 8 2007), 4640-4652.

[23]. Schiller, S., Goedicke, K., Reschke, J., Kirchhoff, V., Schneider, S. and Milde, F. Pulsed magnetron sputter technology. *Surface and Coatings Technology*, 61, 1-3 1993), 331-337.

[24]. Belkind, A., Freilich, A., Lopez, J., Zhao, Z., Zhu, W. and Becker, K. Characterization of pulsed dc magnetron sputtering plasmas. *New Journal of Physics*, 7, 1 2005), 90-90.

[25]. Karthikeyan, S., Hill, A. E., Cowpe, J. S. and Pilkington, R. D. The influence of operating parameters on pulsed D.C. magnetron sputtering plasma. *Vacuum*, 85, 5 2010), 634-638.

[26]. Jung, M. J., Jung, Y. M., Shaginyan, L. R. and Han, J. G. Polycrystalline Si thin film growth on glass using pulsed d.c. magnetron sputtering. *Thin Solid Films*, 420-4212002), 429-432.

[27]. Bartzsch, H., Frach, P. and Goedicke, K. Anode effects on energetic particle bombardment of the substrate in pulsed magnetron sputtering. *Surface and Coatings Technology*, 132, 2–3 2000), 244-250.

[28]. Al-Houty, L., Kassem, M. E. and Abdel Kader, H. I. Variation of the optical energy gap with γ-radiation and thickness in Bi-thin films. *Journal of Materials Science: Materials in Electronics*, 6, 1 1995), 17-20.